Micromechanical measurements of local plastic events in granular materials

Jie Zheng and Aile Sun
School of Physics and Astronomy, Shanghai Jiao Tong University, Shanghai 200240, China

Jie Zhang *
School of Physics and Astronomy, Shanghai Jiao Tong University, Shanghai 200240, China
and Institute of Natural Sciences, Shanghai Jiao Tong University, Shanghai 200240, China

(Received 28 April 2023; revised 30 September 2023; accepted 25 March 2024; published 9 April 2024)

Understanding the interplay between micromechanics and macroscopic plastic deformation in amorphous solids like granular materials is vital. In our study, we directly measured T1 events and associated microscopic stresses in densely packed assemblies of photoelastic disks with varying interparticle friction under pure shear. Our findings demonstrate the existence of T1 events in granular materials under shear, where the statistics of T1 events show a strong correlation with the global shear stress to pressure ratio, and these behaviors are independent of interparticle friction. By dividing T1 events into five categories, we can demonstrate how changes in friction affect their local structure and stability. This provides valuable information about the unique features of T1 events in granular materials, which differ from those in metallic glasses and other frictionless amorphous solids. Additionally, our exploration reveals unique characteristics in the local stresses of T1 events, distinct from frictionless systems like emulsions. Collectively, these findings highlight how interparticle friction modulates the micromechanical properties of T1 events and how their statistical behavior intricately links with the macromechanical responses of granular materials under shear forces.

DOI: 10.1103/PhysRevMaterials.8.045801

I. INTRODUCTION

In contrast to crystalline solids, understanding the deformation of amorphous materials, such as granular substances, colloids, and bulk metallic glasses, remains a topic of considerable debate and investigation [1–20]. While consensus on their predictability in advance remains elusive, it is widely acknowledged that the plastic deformation and the overall stress-strain behavior of amorphous materials are intricately interconnected with the elementary plastic units [2,5,20–36]. For instance, in a two-dimensional (2D) bubble or emulsion system, the elementary plastic event involves the topological exchange of positions among four particles, known as a T1 event [37–39], which occurs when nearest and second-nearest neighbors swap positions. Statistically, it has been observed that the number of T1 events correlates with global stress fluctuations within the bubble system [37]. However, in the case of granular materials, the precise definition of a plastic unit is still a subject of heated debate, primarily due to the influence of interparticle friction [24,40,41].

Furthermore, most theoretical models operate under the assumption that understanding the microscopic plastic behavior and its corresponding mechanical attributes is pivotal for elucidating the macroscopic plasticity of a system. However, in numerous experimental investigations involving foam or bubble systems [37,42], colloids [25], emulsions [38,43,44], and granular systems [45–47], information about the micromechanical characteristics of plastic units and the detailed statistics of local stresses is often conspicuously absent. Additionally, the role of interparticle friction remains an unresolved concern within many theoretical frameworks. Consequently, the interplay between plastic units and interparticle friction in granular materials, and how they influence one another, represents a critical area of exploration. Hence, it becomes imperative to obtain direct experimental evidence of microscopic plastic events and their associated mechanical characteristics, especially under the influence of interparticle friction. This endeavor is essential for gaining profound insights into the deformation mechanisms of amorphous systems, particularly in the context of granular materials.

In this study, we directly measure T1 events [see Fig. 1(a)], representing topological rearrangements of particles, along with associated microscopic stresses in densely packed assemblies of photoelastic disks characterized by varying levels of interparticle friction (denoted as μ) under pure shear. Our findings reveal a striking connection between the evolution of the number of T1 events and the global stress-strain relationship, irrespective of the specific values of μ. The dynamic equilibrium established by the competing processes of T1 event birth and death becomes particularly pronounced post-yield strain, exerting a substantial influence on the overall plastic behavior. However, several systematic quantitative changes emerge as a result of variations in μ.

As μ increases from 0.1 to 0.7 during steady-state shear, the global shear stress-to-pressure ratio $(\tau/P)_G$ rises from approximately 0.22 to 0.27. Simultaneously, the total T1 events decrease from roughly 45% to 30% of the particle count.

*jiezhang2012@sjtu.edu.cn

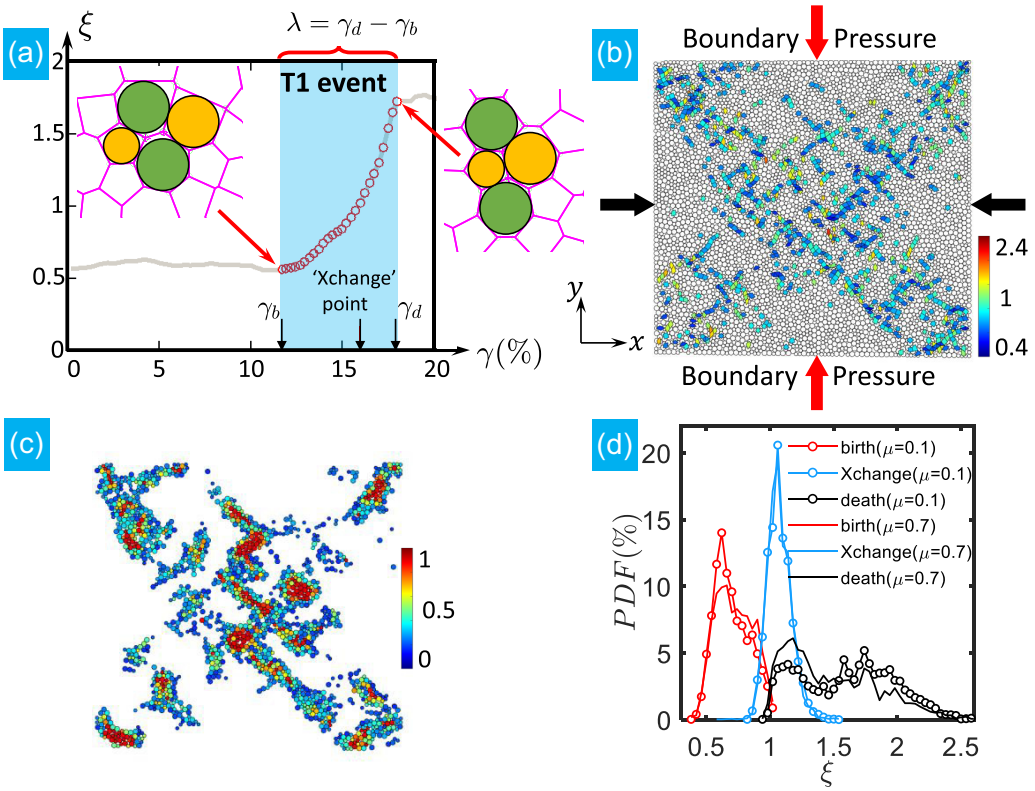

FIG. 1. (a) The evolution of the aspect ratio, denoted as ξ, with the applied strain, denoted as γ, to elucidate key characteristics of T1 events. These characteristics include the birth strain, denoted as γ_b, the "Xchange" point, the death strain, denoted as γ_d, and consequently, the lifetime, represented as λ (defined as $\gamma_d - \gamma_b$). An accompanying inset presents a visual depiction of the two states of a T1 event before and after the exchange of neighboring disk pairs. (b) A schematic of a bidisperse photoelastic disk packing undergoing pure shear. This entails applying compression along the x direction while permitting unimpeded expansion along the y direction under a constant boundary pressure. A snapshot at a strain level of $\gamma = 2\gamma_y$ showcases tracked T1 events, which are illustrated using quadrilaterals connecting the centers of four adjacent particles. The filled colors within these quadrilaterals indicate the instantaneous values of ξ for individual T1 events. (c) Spatial distribution of particles with significant $D^2_{\min}$ values (top 30%). The colors filled in the diagram indicate the degree of nonaffine magnitude associated with the particles. Note that (b) and (c) represent the same global strain state. (d) The PDFs of ξ in three distinct states of T1 events: birth, Xchange, and death. These statistics are derived from aggregating data across T1 events from 8 to 10 realizations for systems characterized by two distinct interparticle friction coefficients, specifically $\mu = 0.1$ and $\mu = 0.7$, respectively.

Moreover, T1 events are divided into distinct categories to gain insight into the unique features of T1 events caused by interparticle friction in granular materials, as opposed to frictionless amorphous systems. We categorize T1 events based on the number of broken bonds in the quadrilateral formed by four adjacent particles involved. With increasing μ, there is a decline in T1 events with zero broken bonds and an increase in those with at least one broken bond, especially for one or two broken bonds, aligning with enhanced shear-induced dilation in high-friction systems. Remarkably, for $\mu = 0.7$, T1 events with one broken bond surpass those with zero broken bonds. Moreover, we find substantial fluctuations in local stresses within T1 events throughout strain evolution. The distributions of local shear stress (τ), local pressure (P), and τ/P ratio remain nearly identical across T1 event states (birth, exchange, and death), but their width and peak are influenced by interparticle friction. Regional averaged stresses show weak dependence on particle locations, distinguishing between T1's core and surrounding particles. Regional averaged pressure is independent of interparticle friction, while regional averaged shear stress is influenced by interparticle friction. Further advancements in plastic theories of granular matter may gain valuable physical insight from these results.

II. EXPERIMENTAL SETUP

We utilized a 2D pure shear system [see Fig. 1(b)] detailed in Ref. [48]. The setup involved a rectangular frame subjected to compression along the x axis and expansion along the y axis, while maintaining constant confining pressure via an air-bearing device. Within the frame, photoelastic particles with diameters of 1 cm (large) and 0.7 cm (small) were immersed in density-matched brine to minimize base friction. Compression along the x axis was applied incrementally in steps of $\delta\gamma = 0.28\%$ for up to 80 strain steps, starting from an initial isotropic jammed state. At each strain step, we recorded particle configurations and stress images using two Nikon cameras. Interparticle contact forces were measured accurately from stress images [48–53], allowing us to construct particle-scale and global stress tensors [48,53,54].

We can first define the Cauchy stress tensor of an individual particle, $\sigma_i \equiv \frac{1}{S_i}\sum_j \mathbf{r}_{ij} \otimes \mathbf{f}_{ij}$. Here $\mathbf{r}_{ij}$ is the position vector from

the center of disk i to the contact point between disks i and j, $\mathbf{f}_{ij}$ is the contact force vector between the two disks i and j, S_i is the area of the Voronoi cell of disk i, and the operator $\otimes$ represents the dyadic product of the two vectors. Starting from the particle Cauchy stress tensor, denoted as σ_i, we proceed to construct either the local or global stress tensor by averaging the individual stress tensors over their respective sets of particles. To illustrate, the global stress tensor σ_G is calculated as the average of all individual stress tensors using the formula $\sigma_G = \frac{1}{N}\sum_i \sigma_i$, where N represents the total number of particles. Similarly, the local stress tensor, denoted as σ, is determined by averaging the particle stress tensors over a specific local set. This is expressed as $\sigma_L = \frac{1}{N_L}\sum_i \sigma_i$, where N_L denotes the total number of particles in the local set. For instance, when computing the local stress tensor for a T1 event involving four core particles, the value of N_L would be 4. Let the principal stresses of either σ_G or σ_L be denoted as σ_1 and σ_2. The pressure, denoted as P, is then calculated as $P = \frac{1}{2}(\sigma_1 + \sigma_2)$, while the shear stress, denoted as τ, is obtained as $\tau = \frac{1}{2}|\sigma_1 - \sigma_2|$.

To ensure statistical validity, we conducted 8–10 independent experimental runs under the same protocol, yielding ensemble averages. We explored a range of confining boundary pressures (8.61 N/m to 10.04 N/m and 11.48 N/m) and system sizes (ranging from 500 to 7000 disks) to confirm consistent results. Our presented results pertain to a boundary pressure of 11.48 N/m and a system size of approximately 3500 disks, consisting of equal numbers of large and small disks. To assess the influence of friction, we systematically compared results for interparticle friction coefficients of $\mu \approx 0.1$ (Teflon-wrapped disks) and $\mu \approx 0.7$ (original disks).

III. RESULTS

Our primary goal is to identify T1 events in a 2D granular system undergoing pure shear, given their crucial role as elementary plastic units in 2D bubble, foam, and emulsion systems [37,38,43]. To achieve this, we apply radial Voronoi tessellation to the particle configuration at each strain step. This method allows us to examine clusters of Voronoi cells formed by four neighboring particles, identifying the two nearest neighbors sharing a common edge. We then track topological changes among these four particles within each cluster, denoting the point at which neighbor switching occurs as the Xchange point of the T1 event. (For a visual representation of T1 event evolution, please see movies within the Supplemental Material, SM [55].) Quantitative analysis of the topological exchange process in a T1 event involves examining the aspect ratio ξ, defined as the ratio between the center-to-center distance of the nearest neighbor and that of the next-nearest neighbors. Figure 1(a) illustrates the evolution of ξ for a T1 event, showing its initial stability followed by a steady increase within a specific strain range, ultimately reaching a constant plateau as the global strain γ increases.

We exclude minor ξ fluctuations resulting from mechanical noise (details in SM [55]), defining the steadily rising ξ phase as the T1 event's effective evolution. In Fig. 1(a), this phase's start (γ_b) and end (γ_d) correspond to the T1 event's birth and death. The T1 event's duration, denoted as the strain interval or lifetime, is $\lambda = \gamma_d - \gamma_b$. Figure 1(b)

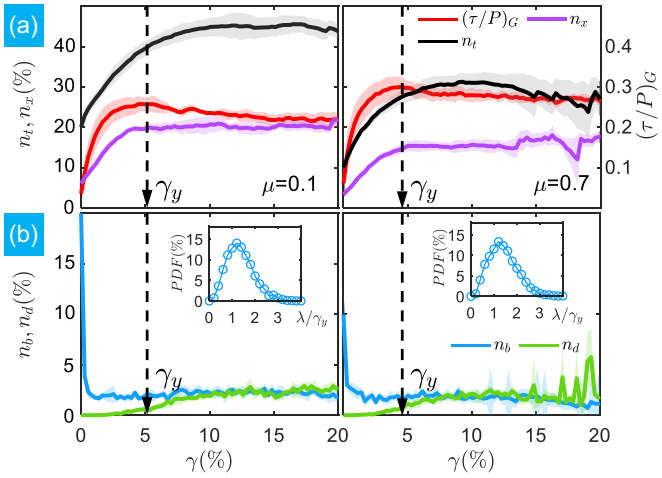

FIG. 2. (a) The total number (n_t) of T1 events, the number of T1 events in the "Xchange" state (n_x), and the global shear stress-to-pressure ratio, denoted as $(\tau/P)_G$, as a function of global strain γ of the system. (b) The number of T1 events at birth (n_b), and the number of T1 events at death (n_d), as a percentage of the particle count, as functions of γ. The insets depict the PDF of the lifetimes, denoted as λ, of T1 events. Notably, λ is rescaled by γ_y. Each panel corresponds to a different frictional system, indicated by $\mu = 0.1$ and $\mu = 0.7$. An arrow is employed to denote the yield strain γ_y, and the shaded area signifies the standard deviation across various realizations.

presents a representative snapshot of the spatial distribution of T1 events at $\gamma = 2\gamma_y$, twice the yield strain γ_y, as the system approaches a steady-state shear. Here γ_y is defined as the strain where the global shear stress to pressure ratio reaches the maximum as shown in Fig. 2(a). T1 events primarily cluster in X-shaped shear bands, consistent with the definition of nonaffine displacement distribution as shown in Fig. 1(c) [23]. Figure 1(d) displays probability distribution functions (PDFs) of ξ at birth, Xchange, and death states, ensemble averaged over all T1 events in the steady-state shear. As expected, the Xchange point distribution exhibits a sharp peak slightly above 1, influenced by bidispersity. Conversely, the PDFs for birth and death states display relatively broad ranges, suggesting that T1 events can exhibit different aspect ratios at their initiation and conclusion. This behavior distinguishes granular systems from bubble and emulsion systems [37,38,43], likely due to the stability of frictional particles and the athermal nature of granular systems [4,54]. Figure 1(d) also shows that the difference in ξ between the two friction systems is not significant.

We now explore the relationship between T1 event characteristics and the macroscopic mechanical behavior of the system, as illustrated by the $(\tau/P)_G$ curve in Fig. 2(a). For better comparison, we present curves depicting the numbers of T1 events at birth (n_b), Xchange (n_x), death (n_d), and the total T1 events (n_t) in Fig. 2. Here the fraction values of $n_t, n_b \ldots$ are obtained from the ratio of nonrepeated counted T1 particles to the total number of particles. We observe that both curves of the $(\tau/P)_G$ and n_x approach steady-state shear at approximately the same strain γ; a qualitative similarity observed for both low $\mu = 0.1$ and high $\mu = 0.7$ interparticle friction. The number of T1 events in the Xchange state,

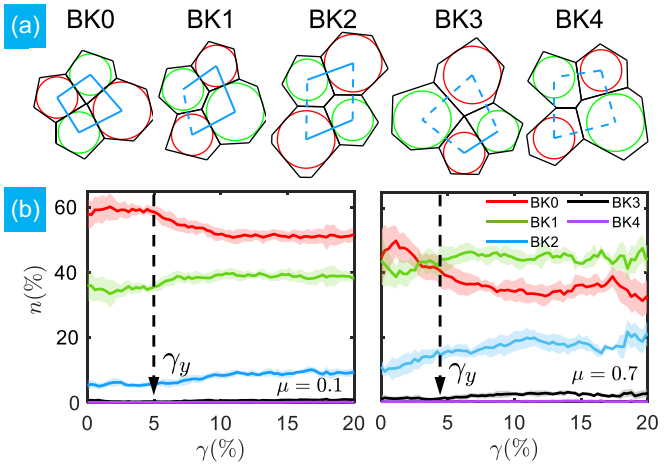

FIG. 3. (a) A schematic illustration showcasing five distinct types of T1 events, where particles are denoted by circles and Voronoi boundaries are represented by black lines. The central blue quadrilateral connects the centroids of four particles, with solid and dashed lines differentiating between the presence and absence of contact between adjacent particles. (b) The percentage distribution of the five types of T1 events as functions of the global strain γ. The two panels correspond to systems of $\mu = 0.1$ and $\mu = 0.7$, respectively. The shaded areas accompanying the graphs represent the standard deviation across various realizations.

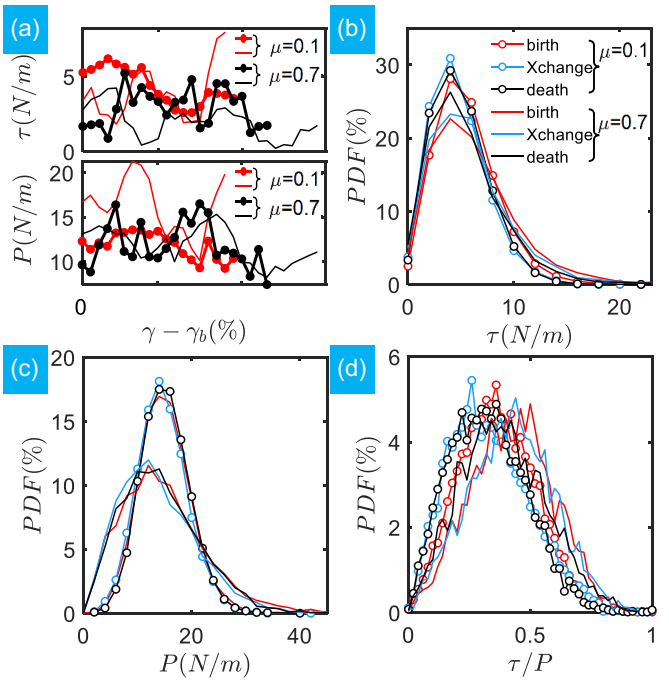

FIG. 4. (a) The transient evolution curves illustrate the local stresses of several representative T1 events. [(b)–(d)] The PDFs for three distinct local properties: local shear stress τ (b), local pressure P (c), and the ratio of τ/P (d). To facilitate comparisons, the PDFs are separately presented for the three stages of T1 events: birth, Xchange, and death. Note that (b)–(d) share a common legend for reference. Furthermore, two different frictional systems characterized by $\mu = 0.1$ and $\mu = 0.7$ are displayed in (b)–(d).

denoted by n_x, is closely correlated with the $(\tau/P)_G$ curve. Both of them increase rapidly and then bend before reaching the yielding point. After that, while n_x starts to stabilize in a steady state, the $(\tau/P)_G$ curve gradually approaches the steady state around the yielding point. The n_b curve drops rapidly to its steady-state value well before reaching γ_y, whereas the n_d curve gradually increases, eventually catching up with n_b. The equilibrium between n_b and n_d occurs after the mechanical yield strain at γ_y, where the $(\tau/P)_G$ curve begins to plateau. However, increasing particle friction leads to a significant decrease in the relative number of T1 events, from approximately $n_t \approx 45\%$ to $n_t \approx 30\%$ of the particle count, while there is a slight increase in global stress from $(\tau/P)_G \approx 0.22$ to $(\tau/P)_G \approx 0.27$ during steady-state shear. Additionally, the PDF of T1 event lifetimes, depicted in the inset of Fig. 2(b), reveals a broad distribution peaking slightly above $\lambda/\gamma_y = 1$. This similar strain scale implies the close connection between global yield strain and the strain duration or lifetime of plastic events. This behavior remains nearly insensitive to μ.

To unveil the profound impact of friction on plastic behavior, we categorize T1 events into five distinct groups, as illustrated in Fig. 3(a), based on the presence or absence of broken contacts (or bonds) among the four edges of neighboring particles. We denote T1 events with no broken bonds as BK0, those with one broken bond as BK1, and those with two broken bonds as BK2, and so forth. Figure 3(b) illustrate the evolving percentages of BK0, BK1-BK4, which gradually reach a plateau after the yield strain γ_y. For $\mu = 0.1$, BK0 predominates, as depicted in the left panel of Fig. 3(b). However, the percentages of BK0 and BK1 switch after γ_y for $\mu = 0.7$, primarily due to enhanced friction-induced stability and shear-induced dilation. Similarly, there is a significant percentage increase in BK2 and BK3 for $\mu = 0.7$ as shown in the right panel of Fig. 3(b). Therefore, T1 events effectively capture frictional effects on micro- and mesoscale plastic deformations in granular materials, as shown in Fig. 3.

Next, our focus shifts to the local stresses of T1 events during steady-state shear. Figure 4(a) presents the erratic evolution of local stress in several typical T1 events, revealing no discernible trend and more supporting evidences are shown in the SM [55]. These findings underscore the significantly more complex nature of local stress relaxation in granular materials, as compared to foam [56] or flowing emulsions [38], where the local shear stress of a T1 event typically exhibits a monotonic increase prior to topological exchange, followed by a continuous decline, and eventually a recovery to its initial level, in accordance with mean field theories [2,3,5,21–23,29,30,32]. To gain deeper insights, we turn to their statistical characteristics in Figs. 4(b)–4(d), which demonstrate that the PDFs of local shear stress (τ), pressure (P), and stress ratio (τ/P) are nearly indistinguishable for the birth, Xchange, and death states of T1 events. Furthermore, these outcomes remain consistent across different friction systems, albeit with broader PDF profiles observed for systems with high friction. These results are robust and independent of the morphology of T1 events, as shown in the SM [55] for details.

To gain insight into the spatial stress properties of T1 events, we compare the evolution of regional averaged stress values among T1 particles, their first surrounding shell of neighbors (N1), the second shell of neighbors (N2), and so

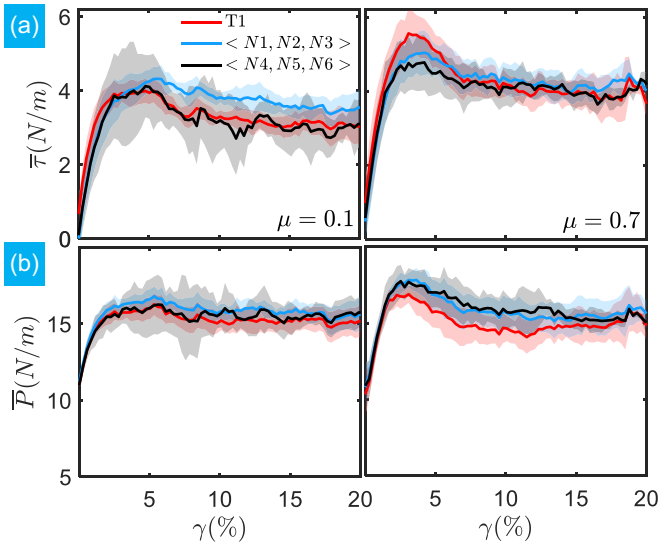

FIG. 5. The regional averaged stresses ($\bar{\tau}$, $\bar{P}$) as functions of γ. To facilitate comparison, we ensemble average the local shear stress (a) and the local pressure (b) over three distinct regions associated with T1 events: T1's four core particles, $\langle N1, N2, N3\rangle$ and $\langle N4, N5, N6\rangle$, where N1, N2, . . . , N6 refer to the first, second, . . . , and sixth shells of particles surrounding T1 events. The shaded areas in the graphs represent the standard deviation computed across 8 to 10 realizations for two different frictional systems, characterized by $\mu = 0.1$ and $\mu = 0.7$, respectively.

forth (N3, . . . , N6) at different strains. To enhance statistical robustness, we group them into three regions: T1 particles as the first region, N1, N2, and N3 as the second region, and N4, N5, and N6 as the third region. Figure 5 reveals that the regional averaged shear stress ($\bar{\tau}$) and pressure ($\bar{P}$) within these three regions are largely similar, with minor deviations that include slightly higher $\bar{\tau}$ in the second region for the $\mu = 0.1$ system and slightly lower $\bar{P}$ in the T1 region for the $\mu = 0.7$ system. Moreover, during steady-state shear, the $\bar{P}$ values remain comparable between low and high μ systems, while the $\bar{\tau}$ values are noticeably higher in $\mu = 0.7$ systems, consistent with the structural characteristics shown in Fig. 3.

IV. DISCUSSION AND CONCLUSIONS

In this study, we conducted micromechanical measurements on densely packed bidisperse photoelastic disks under pure shear, with a specific focus on the statistics and dynamics of T1 events. We observed a close connection between the evolution of T1 events and the stress-strain curve. The interplay between newly created and eliminated T1 events leads to an eventual dynamic equilibrium, a physical scenario applicable across different friction systems. However, quantifiable changes emerge with varying interparticle friction. Increased friction reduces the T1 event count while elevating the relative numbers of broken T1 events.

While nonaffine motion is commonly utilized to examine plastic events in amorphous solids, its spatial distribution resembles that of T1 events, as depicted in Fig. 1. However, the nuanced statistics of T1 events, encompassing birth, exchange, and death, along with associated alterations in the contact network, may not be readily discernible through nonaffine analysis methods. The categorization of T1 events into five distinct groups allows us to explicitly illustrate how variations in interparticle friction impact the local arrangement and stability of T1 events. This offers valuable physical insights into the distinctive characteristics of T1 events in granular materials, distinguishing them from metallic glasses and other amorphous solids. Our findings suggest that T1 events remain instrumental in detecting small- and medium-scale plastic deformations in frictional granular matter, despite their initial development for examining microscopic plastic deformations in metallic glasses and other amorphous materials, such as bubbles and emulsions, which lack interparticle friction.

Furthermore, our extensive research into measuring the local stresses of T1 events has revealed unique characteristics that markedly differ from frictionless systems such as emulsions and foams. In a seminal experiment conducted by Desmond and Weeks, it was observed that in emulsions, the local shear stress of individual T1 events diminishes subsequent to the local rearrangement of the emulsions via T1 events [38]. Consequently, their measured stress propagators exhibit Eshelby-like statistical behavior. Similarly, a comparable relaxation of local stress associated with T1 events has been documented in simulations of dry foam systems [56]. In contrast, T1 events in our frictional granular systems exhibit significant strain-induced local stress fluctuations as shown in Fig. 4, resulting in weak dependencies in the distributions of local stresses for T1 events at birth, during the Xchange phase, and at their conclusion. These distributions are, however, modulated by interparticle friction. Furthermore, the regional averaged stresses in different regions show remarkable similarities. In steady-state shear, the overall pressure level remains independent of interparticle friction, while the overall shear stress level increases with interparticle friction. Our findings underscore the intricate connection between the micromechanical properties of T1 events and the macro mechanical behaviors of granular materials.

Nevertheless, for frictional granular materials, contact sliding and particle rotation operate at length scales below that of T1 events. These mechanisms are of paramount importance in describing material failure at scales below that of individual particles. It is evident that T1 event descriptions are not equipped to directly address material failure at such minute scales. However, our extensive results and analyses, which are based on the statistical behavior of T1 events, demonstrate their capability to effectively capture material failure at mesoscopic scales. Therefore, we contend that the analysis of T1 events holds substantial value in comprehending material failure, at least within the realm of mesoscopic scales. Simultaneously, that delving into the intricate details of contact sliding and particle rotation presents intriguing prospects for our future research.

ACKNOWLEDGMENTS

This work is supported by the NSFC (Grants No. 11974238, No. 12274291, No. 11774221, and No. 12004241). The Innovation Program of Shanghai Municipal Education Commission under Grant No. 2021-01-07-00-02-E00138 also supports this work. We also acknowledge the support from the Student Innovation Center of Shanghai Jiao Tong University.

[1] L. Berthier, G. Biroli, J.-P. Bouchaud, L. Cipelletti, and W. Van Saarloos, *Dynamical Heterogeneities in Glasses, Colloids, and Granular Media* (Oxford University Press, Oxford, 2011).

[2] A. Argon, Acta Metall. **27**, 47 (1979).

[3] P. Sollich, F. Lequeux, P. Hébraud, and M. E. Cates, Phys. Rev. Lett. **78**, 2020 (1997).

[4] H. M. Jaeger, S. R. Nagel, and R. P. Behringer, Rev. Mod. Phys. **68**, 1259 (1996).

[5] M. L. Falk and J. S. Langer, Annu. Rev. Condens. Matter Phys. **2**, 353 (2011).

[6] D. Bonn, M. M. Denn, L. Berthier, T. Divoux, and S. Manneville, Rev. Mod. Phys. **89**, 035005 (2017).

[7] A. Nicolas, E. E. Ferrero, K. Martens, and J.-L. Barrat, Rev. Mod. Phys. **90**, 045006 (2018).

[8] P. Leishangthem, A. D. Parmar, and S. Sastry, Nat. Commun. **8**, 14653 (2017).

[9] S. Sastry, Phys. Rev. Lett. **126**, 255501 (2021).

[10] T. Unger, J. Török, J. Kertész, and D. E. Wolf, Phys. Rev. Lett. **92**, 214301 (2004).

[11] T. Stegmann, J. Török, L. Brendel, and D. E. Wolf, Granul. Matter **13**, 565 (2011).

[12] D. Denisov, K. Lörincz, J. Uhl, K. A. Dahmen, and P. Schall, Nat. Commun. **7**, 10641 (2016).

[13] K. A. Dahmen, Y. Ben-Zion, and J. T. Uhl, Phys. Rev. Lett. **102**, 175501 (2009).

[14] H. G. E. Hentschel, S. Karmakar, E. Lerner, and I. Procaccia, Phys. Rev. E **83**, 061101 (2011).

[15] A. K. Dubey, I. Procaccia, C. A. B. Z. Shor, and M. Singh, Phys. Rev. Lett. **116**, 085502 (2016).

[16] P. K. Jaiswal, I. Procaccia, C. Rainone, and M. Singh, Phys. Rev. Lett. **116**, 085501 (2016).

[17] G. Parisi, I. Procaccia, C. Rainone, and M. Singh, Proc. Natl. Acad. Sci. USA **114**, 5577 (2017).

[18] M. Ozawa, L. Berthier, G. Biroli, A. Rosso, and G. Tarjus, Proc. Natl. Acad. Sci. USA **115**, 6656 (2018).

[19] J. T. Parley, S. Sastry, and P. Sollich, Phys. Rev. Lett. **128**, 198001 (2022).

[20] S. A. Ridout, J. W. Rocks, and A. J. Liu, Proc. Natl. Acad. Sci. USA **119**, e2119006119 (2022).

[21] F. Spaepen, Acta Metall. **25**, 407 (1977).

[22] A. Argon and H. Kuo, Mater. Sci. Eng. **39**, 101 (1979).

[23] M. L. Falk and J. S. Langer, Phys. Rev. E **57**, 7192 (1998).

[24] A. Lemaître, Phys. Rev. Lett. **89**, 064303 (2002).

[25] P. Schall, D. A. Weitz, and F. Spaepen, Science **318**, 1895 (2007).

[26] J. S. Langer, Phys. Rev. E **77**, 021502 (2008).

[27] E. D. Cubuk, S. S. Schoenholz, J. M. Rieser, B. D. Malone, J. Rottler, D. J. Durian, E. Kaxiras, and A. J. Liu, Phys. Rev. Lett. **114**, 108001 (2015).

[28] C. Maloney and A. Lemaitre, Phys. Rev. Lett. **93**, 195501 (2004).

[29] C. E. Maloney and A. Lemaître, Phys. Rev. E **74**, 016118 (2006).

[30] R. Dasgupta, H. G. E. Hentschel, and I. Procaccia, Phys. Rev. Lett. **109**, 255502 (2012).

[31] M. J. Demkowicz and A. S. Argon, Phys. Rev. Lett. **93**, 025505 (2004).

[32] A. Nicolas, J. Rottler, and J.-L. Barrat, Eur. Phys. J. E **37**, 50 (2014).

[33] K. E. Jensen, D. A. Weitz, and F. Spaepen, Phys. Rev. E **90**, 042305 (2014).

[34] S. McNamara, J. Crassous, and A. Amon, Phys. Rev. E **94**, 022907 (2016).

[35] M. Baggioli, I. Kriuchevskyi, T. W. Sirk, and A. Zaccone, Phys. Rev. Lett. **127**, 015501 (2021).

[36] Y. Xing, J. Zheng, J. Li, Y. Cao, W. Pan, J. Zhang, and Y. Wang, Phys. Rev. Lett. **126**, 048002 (2021).

[37] M. Dennin, Phys. Rev. E **70**, 041406 (2004).

[38] K. W. Desmond and E. R. Weeks, Phys. Rev. Lett. **115**, 098302 (2015).

[39] O. Tainio, L. Viitanen, J. R. Mac Intyre, M. Aydin, J. Koivisto, A. Puisto, and M. Alava, Phys. Rev. Mater. **5**, 075601 (2021).

[40] D. Wang, J. Ren, J. A. Dijksman, H. Zheng, and R. P. Behringer, Phys. Rev. Lett. **120**, 208004 (2018).

[41] F. Alonso-Marroquín, I. Vardoulakis, H. J. Herrmann, D. Weatherley, and P. Mora, Phys. Rev. E **74**, 031306 (2006).

[42] G. Debregeas, H. Tabuteau, and J. M. di Meglio, Phys. Rev. Lett. **87**, 178305 (2001).

[43] D. Chen, K. W. Desmond, and E. R. Weeks, Phys. Rev. E **91**, 062306 (2015).

[44] D. Chen, K. W. Desmond, and E. R. Weeks, Soft Matter **8**, 10486 (2012).

[45] A. Amon, V. B. Nguyen, A. Bruand, J. Crassous, and E. Clément, Phys. Rev. Lett. **108**, 135502 (2012).

[46] A. Le Bouil, A. Amon, S. McNamara, and J. Crassous, Phys. Rev. Lett. **112**, 246001 (2014).

[47] N. C. Keim and P. E. Arratia, Phys. Rev. Lett. **112**, 028302 (2014).

[48] J. Zheng, A. Sun, Y. Wang, and J. Zhang, Phys. Rev. Lett. **121**, 248001 (2018).

[49] T. S. Majmudar and R. P. Behringer, Nature (London) **435**, 1079 (2005).

[50] K. E. Daniels, J. E. Kollmer, and J. G. Puckett, Rev. Sci. Instrum. **88**, 051808 (2017).

[51] Y. Wang, J. Shang, Y. Wang, and J. Zhang, Phys. Rev. Res. **3**, 043053 (2021).

[52] L. Zhang, J. Zheng, Y. Wang, L. Zhang, Z. Jin, L. Hong, Y. Wang, and J. Zhang, Nat. Commun. **8**, 67 (2017).

[53] Y. Wang, Y. Wang, and J. Zhang, Nat. Commun. **11**, 4349 (2020).

[54] D. Bi, J. Zhang, B. Chakraborty, and R. P. Behringer, Nature (London) **480**, 355 (2011).

[55] See Supplemental Material at http://link.aps.org/supplemental/10.1103/PhysRevMaterials.8.045801 for calculation details of T1 stresses, and comparison of T1 stresses in different evolving states, different types etc. It also includes a video on the evolution of T1 events in the granular system.

[56] A. Kabla and G. Debrégeas, Phys. Rev. Lett. **90**, 258303 (2003).